

RESEARCH ARTICLE

10.1002/2016PA002944

Key Points:

- Bayesian hierarchical regressions are applied to sea surface temperature reconstructions
- Local sea surface temperature response to eight climate indicators is estimated for 54 reconstructions
- “Universal curve” of change in sea surface temperature by latitude is stable over 400,000 years

Supporting Information:

- Supporting Information S1
- Data Set S1

Correspondence to:

C. W. Snyder,
Carolyn.snyder@gmail.com

Citation:

Snyder, C. W. (2016), Bayesian hierarchical regression analysis of variations in sea surface temperature change over the past million years, *Paleoceanography*, 31, 1283–1300, doi:10.1002/2016PA002944.

Received 26 FEB 2016

Accepted 29 AUG 2016

Accepted article online 6 SEP 2016

Published online 23 SEP 2016

Bayesian hierarchical regression analysis of variations in sea surface temperature change over the past million years

Carolyn W. Snyder¹

¹Interdisciplinary Program in Environment and Resources, Stanford University, Stanford, California, USA

Abstract Statistical challenges often preclude comparisons among different sea surface temperature (SST) reconstructions over the past million years. Inadequate consideration of uncertainty can result in misinterpretation, overconfidence, and biased conclusions. Here I apply Bayesian hierarchical regressions to analyze local SST responsiveness to climate changes for 54 SST reconstructions from across the globe over the past million years. I develop methods to account for multiple sources of uncertainty, including the quantification of uncertainty introduced from absolute dating into interrecord comparisons. The estimates of local SST responsiveness explain 64% (62% to 77%, 95% interval) of the total variation within each SST reconstruction with a single number. There is remarkable agreement between SST proxy methods, with the exception of Mg/Ca proxy methods estimating muted responses at high latitudes. The Indian Ocean exhibits a muted response in comparison to other oceans. I find a stable estimate of the proposed “universal curve” of change in local SST responsiveness to climate changes as a function of $\sin^2(\text{latitude})$ over the past 400,000 years: SST change at 45°N/S is larger than the average tropical response by a factor of 1.9 (1.5 to 2.6, 95% interval) and explains 50% (35% to 58%, 95% interval) of the total variation between each SST reconstruction. These uncertainty and statistical methods are well suited for application across paleoclimate and environmental data series intercomparisons.

1. Introduction

Most research on global paleoclimatic temperature patterns has focused on detailed reconstructions of single points in time, such as the Last Glacial Maximum (LGM, 19–23 kyr ago) [e.g., *Climate: Long-Range Investigation, Mapping, and Prediction (CLIMAP) Project Members*, 1981; *Multiproxy approach for the reconstruction of the glacial ocean surface (MARGO) Project Members*, 2009]. Research results based on a single time slice, however, may not be generalizable beyond their particular point in time. Such research also assumes that functional relationships are linear and estimates their slopes using only two points: the single time slice as compared to the present [e.g., *Rohling et al.*, 2012; *Shakun et al.*, 2012]. Other studies have focused on comparisons of proxy reconstructions from a single ocean core to global climate variables over time [e.g., *Genthon et al.*, 1987; *Lorius et al.*, 1990; *Lea*, 2004]. Single cores also have been used to compare different proxy methods on the same core samples [e.g., *Barrows et al.*, 2007]. Research on single cores, however, cannot investigate spatial patterns and the importance of other core-specific variables.

New databases of proxy records have the potential to provide unique contributions to our understanding of the climate system. Unfortunately, such databases are highly underutilized. Common barriers to intercomparisons among different proxy reconstructions are different timescales, inconsistent representations of uncertainty, and a concern that core-specific differences, such as proxy type, ocean, and latitude, prohibit useful comparisons. Given the potential for large uncertainties in paleoclimate reconstructions, it is imperative that any investigation includes rigorous consideration of uncertainty and robust statistical methods that account for the nature of the latent process and the proxy data. Inadequate consideration of these uncertainties, as well as model misspecification in terms of the nature of the process and/or the data, can result in misinterpretation, overconfidence, and biased conclusions about the climate system.

There is a growing literature that employs Bayesian models to overcome these challenges. *Clark and Gelfand* [2006] discuss a variety of applications of Bayesian hierarchical models across the environmental sciences. For example, *Haslett et al.* [2006] develop a hierarchical Bayesian model to explicitly model uncertainty in

reconstructing climate histories from fossil pollen over the last 12,000 years. Additionally, *Li et al.* [2007, 2010a] employ Bayesian models, bootstrapping, and cross validation to explicitly account for different sources of uncertainty in proxy reconstructions of Northern Hemisphere average temperature over the past thousand years. In another example, *Tingley and Huybers* [2010] develop a hierarchical Bayesian algorithm to assimilate both proxy and instrumental data sets and estimate uncertainty in climate anomalies in time and space. *Tingley et al.* [2012] summarize recent statistical approaches to paleoclimate reconstructions of the past thousand years. Most recently, *Lin et al.* [2014] present a probabilistic stratigraphic alignment algorithm to determine Bayesian confidence intervals for oxygen isotope alignment.

In this research, I extend these Bayesian methods to assess patterns in sea surface temperature (SST) change over the past million years. I investigate the relationship between different SST reconstructions and major climate indicators, quantifying the influences of latitude, ocean, and proxy method on changes in local SST. To explore these questions, I compile a database of SST reconstructions over the past million years, including multiple proxy reconstruction methods (section 2). Uncertainty analysis methods are developed to estimate and propagate several sources of uncertainty in the proxy records (section 3). In order to analyze variations both within a given SST reconstruction as well as between different SST reconstructions, I apply Bayesian hierarchical regressions (section 4). I then discuss major results (section 5) and key conclusions (section 6).

2. Paleoclimate Data

This analysis uses a multiproxy approach to reconstruct sea surface temperature. I develop a SST database from an extensive literature review of hundreds of published SST reconstructions. The database includes SST reconstructions based off geochemical paleothermometers (using alkenone unsaturation indices (U_{37}^k) and ratios of Mg/Ca in planktonic foraminifera) and SST reconstructions based off microfossil abundances (using transfer functions for planktonic foraminifera and radiolarians). A multiproxy approach enables the reduction of the uncertainties and potential biases specific to each proxy method by combining estimates from several independent proxies [*Mix et al.*, 2001; *Li et al.*, 2010b; *Jones et al.*, 2009].

To be included in the database, the reconstructions must have covered at least the past 100 kyr (cal kyr B.P.) with minimum average resolution of 10 kyr. I exclude records that are known to represent extreme local variations and not regional climate changes per literature or have significant quality concerns raised in the literature. I supplement this literature review with an investigation of the adjusted R^2 of each SST reconstruction with Antarctic temperature deviations [*Jouzel et al.*, 2007], using a low threshold of R^2 equal to 0.2 to indicate the need for further investigation. I exclude records that have been contradicted and criticized in the literature. Where possible, I update older reconstructions with more recent and widely accepted calibration equations. The final SST database includes 54 SST reconstructions: 23 from alkenone indices, 16 from species assemblages methods, and 15 from Mg/Ca ratios (Figure 1, Table 1, and Data Set S1 in the supporting information). There are a total of 12,105 point reconstructions of SST. It is important to note that the records have limited geographical distribution, variable length, and variable resolution. The following discussion summarizes the critical uncertainties for each proxy method to illustrate the drivers of the uncertainty estimates.

Alkenones are sedimentary organic molecules (specifically long-chained unsaturated ethyl and methyl ketones) produced by some haptophyte algae in open marine waters. The relative abundances of unsaturated forms of alkenones (represented in alkenone indices, U_{37}^k) are thought to reflect seawater temperature during their production. Some potential limitations of alkenone indices as SST proxies include the following: nonlinear responses at high and low temperature extremes [*Mix et al.*, 2001; *Bard*, 2001]; bioturbation and redeposition [*Mix et al.*, 2001; *Barrows et al.*, 2007]; peak production at subsurface depths, in seasonal blooms, and/or related to nutrient flows and upwelling [*Mix et al.*, 2001; *Barrows et al.*, 2007; *Horikawa et al.*, 2006; *Weldeab et al.*, 2007a; *Seki et al.*, 2007]; and the lack of understanding of the use and synthesis of alkenones [*Gonzalez et al.*, 2001]. At high latitudes, the seasonality of alkenone production seems to be more pronounced, and the reconstructed SST at high latitudes is thought to be more representative of summer than mean annual growth conditions [*Mix et al.*, 2001; *Weaver et al.*, 1999; *Bard*, 2001].

The Mg/Ca ratio in biogenic calcite from foraminifera shells varies systematically with the seawater temperature at calcification. The Mg/Ca ratios can be used to calculate both SST and deep water temperature from planktonic and bottom-dwelling foraminifera, respectively. Some potential limitations of Mg/Ca ratios as SST proxies are differential dissolution and secondary growth [*Mix et al.*, 2001; *Brown and Elderfield*, 1996],

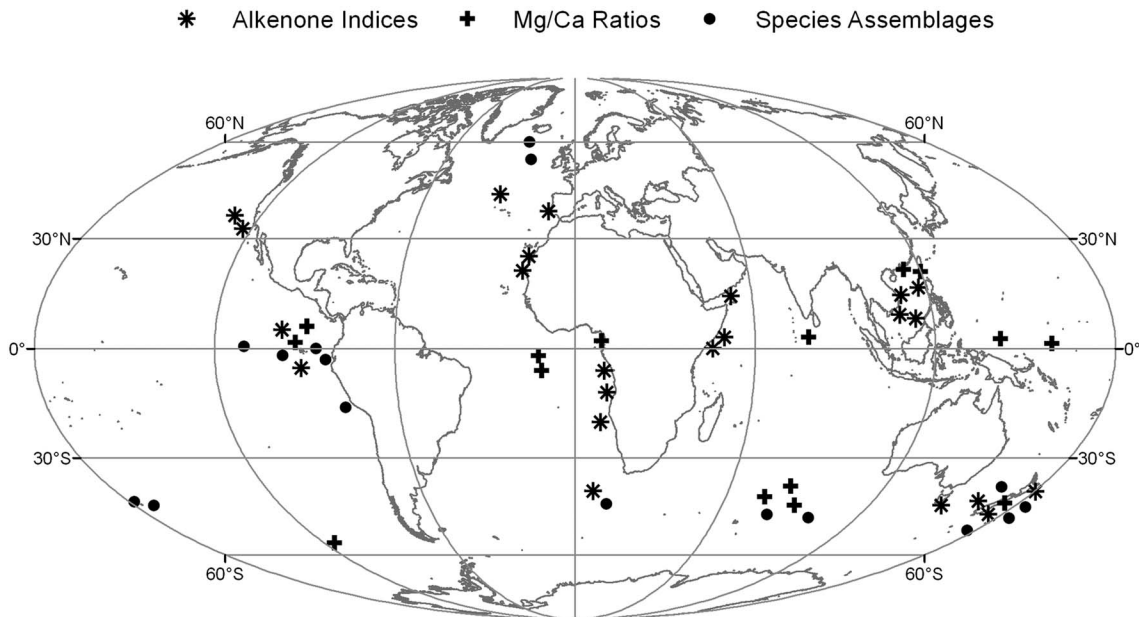


Figure 1. Distribution in space of the 54 SST proxy reconstructions used in this analysis (see section 2 and Table 1). The shapes indicate the SST proxy method: alkenone indices in asterisks, Mg/Ca ratios in plus signs, and species assemblages methods in solid circles.

Table 1. Database of Paleoclimate Reconstructions

Record	Citation	Latitude	Longitude	Start Date (yr B.P.)	End Date (yr B.P.)
<i>Alkenone Indices SST Proxy Reconstructions</i>					
1	Bard [2002]	38°N	10°W	0	110,100
2	Bard et al. [1997]	0°S	46°E	0	151,500
3	Bard et al. [1997]	3°N	50°E	0	149,200
4	Clemens et al. [2008]	19°N	116°E	4,178	4,690,916
5	Eglinton et al. [1992]	21°N	18°W	736	653,042
6	Horikawa et al. [2006]	0°N	95°W	1,100	154,097
7	Lawrence et al. [2006]	3°S	91°W	5,230	5,089,802
8	Müller et al. [1997]	20°S	9°E	3,300	402,900
9	Pahnke and Sachs [2006]	46°S	175°E	1,950	156,360
10	Pahnke and Sachs [2006]	40°S	178°E	3,320	135,050
11	Pelejero et al. [1999]	15°N	111°E	0	221,100
12	Pelejero et al. [1999]	8°N	112°E	0	142,290
13	Pelejero et al. [2006]	42°S	170°E	3,570	288,540
14	Pelejero et al. [2006]	44°S	150°E	5,045	459,632
15	Rostek et al. [1997]	14°N	53°E	2,300	152,600
16	Sachs and Anderson [2003]; Pahnke and Sachs [2006]	41°W	9°E	6,080	160,000
16	Schneider et al. [1995]	6°S	10°E	400	189,000
17	Schneider et al. [1995]	12°S	11°E	1,300	200,600
19	Sicre et al. [2000]	25°N	16°W	5,000	144,000
20	Villanueva et al. [1998]	43°N	30°W	2,900	285,900
21	Yamamoto et al. [2004]; Yamamoto et al. [2007]	32°N	119°W	870	157,048
22	Yamamoto et al. [2004]; Yamamoto et al. [2007]	34°N	122°W	3,186	136,475
23	Zhao et al. [2006]	9°N	110°E	905	148,886
<i>Mg/Ca Ratio SST Proxy Reconstructions</i>					
24	de Garidel-Thoron et al. [2005]	2°N	142°E	7,000	1,755,000
25	Lea [2004]	2°N	91°W	1,000	361,000
26	Lea et al. [2006]	0°N	92°W	1,200	135,100

Table 1. (continued).

Record	Citation	Latitude	Longitude	Start Date (yr B.P.)	End Date (yr B.P.)
27	<i>Mashiotta et al.</i> [1999]	43°S	80°E	2,700	293,700
28	<i>Mashiotta et al.</i> [1999]	56°S	115°W	8,110	108,450
29	<i>Medina-Elizalde and Lea</i> [2005]	0°N	159°E	4,300	1,348,000
30	<i>Nürnberg et al.</i> [2000]	2°S	12°W	240	274,630
31	<i>Nürnberg et al.</i> [2000]	6°S	11°W	1,000	271,000
32	<i>Oppo and Sun</i> [2005]	20°N	118°E	1,943	142,571
33	<i>Pahnke et al.</i> [2003]	45°S	175°E	1,951	340,835
34	<i>Rickaby and Elderfield</i> [1999]	40°S	85°E	4,750	196,710
35	<i>Rickaby and Elderfield</i> [1999]	44°S	90°E	3,600	283,670
36	<i>Saraswat et al.</i> [2005]	3°N	78°E	5,434	137,333
37	<i>Wei et al.</i> [2007]	20°N	117°E	1,740	261,300
38	<i>Weldeab et al.</i> [2007b]	2°N	9°E	360	155,420
<i>Species Assemblages SST Proxy Reconstructions</i>					
39	<i>Barrows et al.</i> [2007]	42°S	170°E	3,830	142,712
40	<i>Barrows et al.</i> [2007]	46°S	175°E	5,401	133,995
41	<i>Brathauer and Abelmann</i> [1999]	43°S	12°E	387	338,519
42	<i>Kandiano et al.</i> [2004]	54°N	20°W	2,375	193,065
43	<i>Labeyrie et al.</i> [1996]; <i>Rickaby and Elderfield</i> [1999]	46°S	96°E	4,590	149,250
44	<i>Martinson et al.</i> [1987]	44°S	80°E	750	294,000
45	<i>Pisias and Mix</i> [1997]	0°N	96°W	360	752,047
46	<i>Pisias and Mix</i> [1997]	3°S	83°W	1,914	151,051
47	<i>Pisias and Mix</i> [1997]	0°N	110°W	880	144,763
48	<i>Pisias and Mix</i> [1997]	0°N	86°W	1,479	154,653
49	<i>Pisias and Mix</i> [1997]	16°S	78°W	785	466,520
50	<i>Weaver et al.</i> [1998]	44°S	172°W	0	170,000
51	<i>Weaver et al.</i> [1998]	46°S	172°E	0	116,705
52	<i>Weaver et al.</i> [1998]	45°S	179°E	170	120,880
53	<i>Weaver et al.</i> [1998]	43°S	178°W	0	154,600
54	<i>Weaver et al.</i> [1999]	60°N	23°W	0	120,000
<i>Climate Indicators</i>					
c1	<i>Jouzel et al.</i> [2007]	75°S	123°E	38	801,662
c2	<i>Cuffey and Vimeux</i> [2001]	78°S	107°E	400	350,000
c3	<i>Kawamura et al.</i> [2007]	77°S	39°E	750	339,500
c4	<i>Masson-Delmotte et al.</i> [2005]	73°N	38°W	100	100,000
c5	<i>Masson-Delmotte et al.</i> [2006]	75°N	42°W	0	122,400
c6	<i>Lüthi et al.</i> [2008]	composite	composite	137	798,512
c7	<i>Lüthi et al.</i> [2008]; <i>Loulergue et al.</i> [2008]	composite	composite	13	799,396
c8	<i>Lisiecki and Raymo</i> [2005]	composite	composite	0	5,320,000

the cleaning and measurement procedures [Mix et al., 2001; Barker et al., 2003; Lea et al., 2005; Weldeab et al., 2006], uncertain calcification depth and timing [Anand et al., 2003; Kucera et al., 2005a; Regenberg et al., 2009], and complications by pH, salinity, upwelling, and species-specific effects [Mix et al., 2001; Elderfield and Ganssen, 2000; Lea et al., 1999; Nürnberg et al., 2000; Robinson et al., 2008]. High-latitude SST reconstructions with Mg/Ca ratios have also found significant bias and uncertainty, including a tendency to under predict variations [Kandiano et al., 2004; Barker et al., 2005; Meland et al., 2005].

SST reconstructions estimated from microfossils abundances use a variety of empirical statistical methods, with the common assumption that the modern spatial patterns of species abundance are controlled by the

same mechanisms that control changes through time at any site [Mix *et al.*, 2001; Birks *et al.*, 2010]. Recent research supports using a combination of analytical methods to reduce overall bias and assess reliability [Kucera *et al.*, 2005b; Barrows *et al.*, 2007]. SST reconstructions from species abundance are potentially limited by the lack of a suitable modern analog for some geologic samples, the lack of understanding of the ecology of each fossil group, the effects of interdependent environmental variables, the bioturbation of modern core tops, and dependence on the calibration data set [Mix *et al.*, 2001; Kucera *et al.*, 2005a, 2005b; Birks *et al.*, 2010; Robinson *et al.*, 2008; Telford *et al.*, 2013]. Species abundance reconstructions of SST tend to be inherently more noisy than geochemical reconstructions because of the presence of variables other than temperature that influence species abundances [Barrows *et al.*, 2007]. Moreover, the planktonic foraminifera assemblage data may reflect subsurface temperature not SST [Telford *et al.*, 2013]. When more than one SST reconstruction is available from species abundance methods, I analyze separately the different analytical methods and warm/cold season outputs and find that the regression coefficient estimates are not significantly different from each other. Therefore, I use a single-average compiled SST reconstruction with a variance estimate covering the different seasons and methods.

In addition to the SST proxy records, eight different paleoclimate records that are thought to be indicators of major climate changes are included for comparison (Table 1): polar temperature reconstructions from Antarctica and Greenland using deuterium excess, carbon dioxide radiative forcing and total greenhouse gas (GHG) radiative forcing, and a stack of 57 globally distributed benthic marine records of deep-sea oxygen-18 isotopes. I reconstruct the greenhouse gas radiative forcing estimates from Antarctic ice core gas records for methane and carbon dioxide using the global forcing equations from Hansen *et al.* [2008].

3. Paleoclimate Proxy Uncertainty Quantification

For the local SST proxy reconstructions there are five major sources of uncertainty: (1) error in the direct measurement of the proxy itself; (2) error in the proxy calibration; (3) structural uncertainty in the proxy method; (4) time averaging of the sample, both from natural and sampling processes; and (5) absolute dating uncertainty.

Estimates of the measurement and calibration errors are available from lab and field experiments for the different proxy methods (for example, from alkenone indices [Müller *et al.*, 1998; Herbert, 2001], Mg/Ca ratios [Mashiotta *et al.*, 1999; Elderfield and Ganssen, 2000], and species assemblages [Barrows *et al.*, 2007]) and typically range from 1°C to 3°C for two standard deviations. However, the published uncertainty estimates often do not include considerations of structural uncertainty from the assumptions of the proxy method. For example, the proxy calibration process assumes that the relationship found today will hold for the different climatic and chemical conditions of the past. However, evolution and other environmental changes could produce different relationships in the past than found in the present. Another assumption is that the only variable that would cause changes in the proxy value is the particular variable of interest, because otherwise changes in other variables could bias the inferences (social scientists call this effect “omitted variable bias”). Therefore, I use the upper range of the published values of 3°C (95% interval) as an estimate for the combined uncertainty for each of the SST proxy methods.

It is imperative that comparisons between paleoclimate records include the uncertainty in matching which parts of each record occurred at the same point in time [Haam and Huybers, 2010; Lin *et al.*, 2014; Breitenbach *et al.*, 2012; Werner and Tingley, 2015]. Dating uncertainty can be a significant limitation, especially for comparisons of periods of rapid change or analyses of leads and lags of different variables. Few studies have analyzed the effects of dating uncertainty, and even fewer have propagated the dating uncertainty in their reconstructions and analyses [Lin *et al.*, 2014]. Here I develop a technique to estimate the contribution of such uncertainty to interrecord comparisons using nonparametric regressions, enabling such uncertainty to be propagated in a full uncertainty analysis. I use the estimate of 10 kyr (95% interval) for dating uncertainty from orbital tuning [Martinson *et al.*, 1987; Huybers and Wunsch, 2004; Huybers, 2007; Lin *et al.*, 2014], unless papers provide specific estimates of uncertainty in their timescales.

When comparing independent records, $a(t_p)$ and $b(t_q)$, using uncertain absolute timescales, it is necessary to estimate $a(t_p)$ at t_q , called \hat{a}_q . To estimate \hat{a}_q , I take a weighted average of the time series $a(t_p)$ around the time point t_q . The amount of dating uncertainty in $b(t_q)$, called $s_{t(q)}$, sets the breadth of sampling around the time point t_q : greater dating uncertainty means wider sampling of $a(t_p)$. Weights for the weighted average, ω_{pq} ,

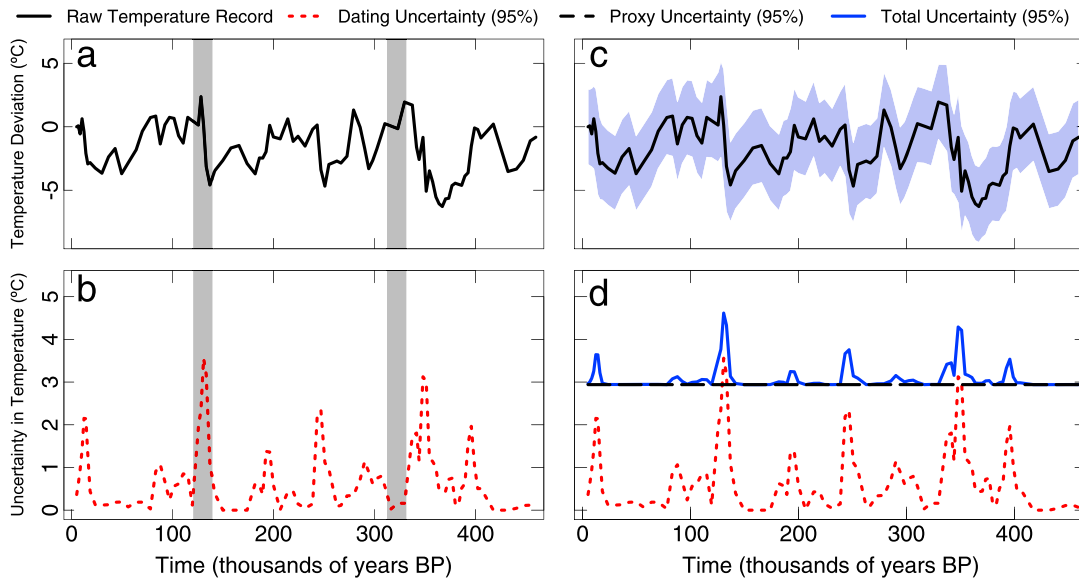


Figure 2. Illustration of combining estimates of both proxy uncertainty and dating uncertainty for a proxy reconstruction. (a, c) The raw Antarctica Dome Concordia temperature deviation record as a solid black line [Jouzel *et al.*, 2007]. (b, d) The estimated uncertainty (section 3) due to a timescale uncertainty of 10,000 years (95% interval), which is typical for SST reconstructions, is shown as a dotted red line. Note that the high uncertainty in temperature from dating uncertainty arises during times of rapid temperature change in the record, whereas periods of relatively stable temperature have low associated uncertainty from dating error (see shaded periods for examples). Figure 2d shows the proxy uncertainty in polar temperature reconstruction of 3°C (95% interval), which is constant over time, in a dashed black line. The two sources of uncertainty (proxy and dating) are summed as variances and displayed as the solid blue line in Figure 2d and the blue shading in Figure 2c (95% interval).

are determined based on the distance in time between t_p and t_q , and the bandwidth parameter, h_q , is equal to $s_{t[q]}$: the closer to time t_q , the more heavily weighted the data point.

$$\hat{a}_q = \sum_{p=1}^n \omega_{pq} a_p \quad (1)$$

$$\omega_{pq} = \phi_q(t_p) / \sum_{p=1}^n \phi_q(t_p) a_p \quad (2)$$

$$\phi_q(t_p) = (2\pi h_q^2)^{-0.5} * \exp \left[- (t_p - t_q)^2 / 2h_q^2 \right] \quad (3)$$

A similar method is used to estimate the uncertainty in the estimate of \hat{a}_q , variance $\hat{s}_{a[q]}^2$. I estimate the weighted average of the squared difference between every point in $a(t_p)$ and the estimated \hat{a}_q , called the residuals; \hat{r}_{pq}^2 are equal to $(a_p - \hat{a}_q)^2$. The weights are the same as before. This method is a local constant simplification of the method discussed by Fan and Yao [1998] for the estimation of conditional variance functions in stochastic regression.

$$\hat{s}_{a[q]}^2 = \sum_{p=1}^n \mu_{pq} \hat{r}_{pq}^2 \quad (4)$$

$$\mu_{pq} = \phi_q(t_p) \sum_{p=1}^n \phi_q(t_p) \hat{r}_{pq}^2 \quad (5)$$

This method is implemented using the Nadaraya-Watson kernel-weighted local constant regression modified to include a locally varying bandwidth, using the function “ksmooth” in the R statistical program (<http://stat.ethz.ch/R-manual/R-patched/library/stats/html/ksmooth.html>); see Text S1. The method allows the bandwidth to vary by time point, which is essential for the many reconstructions whose dating uncertainty increases for samples farther back in time, causing heteroscedasticity in the dating error. Rehfeld *et al.* [2011] support the use of Gaussian kernels as a reliable and more robust estimate for dealing with irregular sampling. Figure 2 shows the results for a single record and illustrates how periods of rapid temperature change in the record dating uncertainty can increase total uncertainty by over 50%.

A limitation of this method is that it does not include the unidirectional nature of time. Unless there was depositional disturbance, one can be confident that shallower deposits are younger than deeper deposits and thus both time and deposition are unidirectional in nature. In other words, we know that measurements deeper down in the ocean core are older than the shallower measurements and this should constrain our estimates of uncertainty in a time series. Therefore, this method may be overly conservative in its uncertainty estimation results.

Kheshgi and Lapenis [1996] also identified the importance of translating dating errors into temperature errors before comparing different reconstructions, but their proposed method necessitated assumptions about the distribution of temperature variability. In contrast, the method described here allows dating uncertainty to vary by time point in each record and does not assume variability characteristics.

Breitenbach et al. [2012] develop a software package, COPRA1.0, that uses a Monte Carlo simulation to translate dating uncertainties to uncertainties in the proxy values, leveraging absolute dating points, layer counting, and/or marker boundaries. In many ways, this paper's method is a simplification of the approach of *Breitenbach et al.* [2012], similarly focused on transferring the dating uncertainty into the SST uncertainty at a certain time point and using a weighted average around the time point to do so. The one exception is that the Breitenbach method does not have the limitation as noted above of not preserving the unidirectional nature of time. However, the reconstructions used by this research do not have sufficient dating estimates for the method, because most of the age scales are based on orbital tuning. In addition, *Werner and Tingley* [2015] use a Bayesian hierarchical reconstruction model to quantify uncertainty across multiple possible age models, with a focus on reconstructions and dating resources available over the last 2 kyr.

For the records in this analysis, the estimated amount of time averaging is significantly less than the estimated uncertainty in absolute age. Had this not been the case, all records could have been first smoothed to the same amount of time averaging using the Nadaraya-Watson kernel-weighted local constant regression, as described above, with the larger time-averaging range taken as the 95% interval for the smoothing bandwidth.

I assume that the various sources of uncertainty are independent, and thus, I sum variances to propagate errors. I convert each SST reconstruction into a deviation by subtracting the mean SST of each record over the past 100 kyr (the longest period that all the records share) to minimize artifacts due to absolute temperature variations between SST reconstructions. Figure 2 illustrates the full estimate of temperature uncertainty that includes both estimates in proxy uncertainty and dating uncertainty.

4. Statistical Methods

4.1. Traditional Statistical Approach

To assess patterns in SST change within and between different SST reconstructions, a variable termed "local SST responsiveness" is defined and estimated. Local SST responsiveness is the change in SST at a particular ocean core relative to changes in a "standard" record. In this research, paleoclimatic reconstructions that are thought to indicate global/major climate changes serve as the standard record of comparison. Eight different climate indicators are used to quantify the methodological uncertainty associated with the choice of indicator record (section 2). This concept is analogous to *Rohling et al.'s* [2012] estimates of "mean long-term linear temperature response" in their investigations of climate sensitivity.

Figure 3 shows example scatterplots of changes in local SST to changes in GHG radiative forcing. The slope of the linear relationship of change in local SST to change in GHG radiative forcing is the local SST responsiveness and can be assessed through a linear regression. For one SST reconstruction, the regression of change in SST as a function of change in a climate indicator can be assessed using a weighted least squares regression with estimates of uncertainty in the SST proxy reconstructions:

$$\hat{y}_t \sim N(X_t \beta, \hat{\sigma}_{y_t}^2) \tag{6}$$

where t is time, \hat{y}_t is the change in SST at time t (single value), X_t is the change in the climate indicator at time t (single value), β is the local responsiveness of SST reconstruction to the climate indicator (single value), and $\hat{\sigma}_{y_t}^2$ is the variance for the predicted \hat{y}_t value (single value).

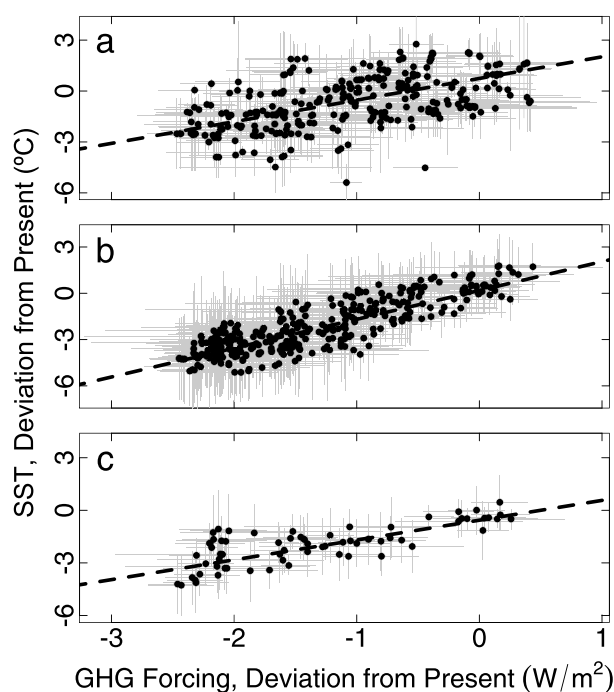


Figure 3. Examples of simple regression analyses of changes in GHG radiative forcing on the x axis with changes in SST on the y axis from (a) the North Atlantic using alkenone indices [Eglinton *et al.*, 1992], from (b) the South Pacific using Mg/Ca ratios [Pahnke *et al.*, 2003], and from (c) the tropical Pacific using faunal assemblages [Pisias and Mix, 1997]. Each point in the figure represents a single time point, with glacial maxima time points in the lower left corner and interglacial time points in the upper right corner. The grey bars are the 95% intervals estimated from proxy uncertainty and dating uncertainty (see section 3). The black dashed lines are the results from a weighted least squares regression analysis. The slopes of these lines are estimates of the local SST responsiveness for each reconstruction (see Figure 4 for all 54 SST reconstructions).

SST records through independent regression with reconstructions of changes in global radiative forcing over the past 520 kyr.

Local SST responsiveness is found to be an effective summary statistic characterizing the variation in each of the SST reconstructions (see section 5.1 for more discussion). These results spur subsequent questions: how does responsiveness vary by proxy, by time period, by ocean, by longitude, by latitude? A simple approach would be to regress the local SST responsiveness results against SST reconstruction-specific variables, such as proxy method and ocean, using a weighted least squares regression using estimates of uncertainty in the responsiveness estimates:

$$\beta_j \sim N(\mathbf{U}_j \mathbf{G}, \sigma_\beta^2) \quad (7)$$

where j is the index over the 54 SST reconstructions; β_j is the local responsiveness of SST reconstruction j to the climate indicator estimated from independent regressions (single value); \mathbf{U}_j are the reconstruction-specific variables such as proxy method and ocean basin (vector); \mathbf{G} are the coefficients for how the \mathbf{U} variables influence β (vector); and σ_β^2 is the variance for the predicted β value (single value).

The results of such a regression are plotted in Figure 4 and listed in Table S2. The major limitation of this approach is that the sample size (and thus the degrees of freedom) is dramatically reduced to only 54 reconstructions. Such a simplification of the data limits the number of questions and variables that can be explored, especially interactive variables, and also potentially reduces the significance of the results. Moreover, such a strategy would insufficiently characterize the structure of the uncertainty in the estimates, which should

The resulting estimate of local SST responsiveness is plotted for each reconstruction in Figure 4, using GHG radiative forcing as the climate indicator. The adjusted R^2 statistic (Figure 5a) reflects the percent of local SST variation for each reconstruction that is explained by changes in the climate indicator. In addition to a linear relationship, I also test three additional functional relationships: the climate indicator leading by one time step (1 kyr), the climate indicator lagging by one time step (1 kyr), and a quadratic of the climate indicator. I find that the real-time linear relationship is the best fit of the four functional relationships, with fit assessed from the adjusted R^2 estimates. It is worth noting that the time resolution of this analysis (1 kyr) is significantly longer than the typical lead/lag differences discussed in the literature between CO_2 forcing and temperature [e.g., Shakun *et al.*, 2012].

The regressions are then repeated independently for each of the 54 reconstructions against each of the eight climate indicators (the distributions of individual adjusted R^2 estimates are shown in Figure 5b and the regression results are in Table S1). This is a “no pooling” implementation from a Bayesian perspective, because all the SST reconstructions are investigated independently from one another. Rohling *et al.* [2012] performed a similar statistical analysis comparing 36

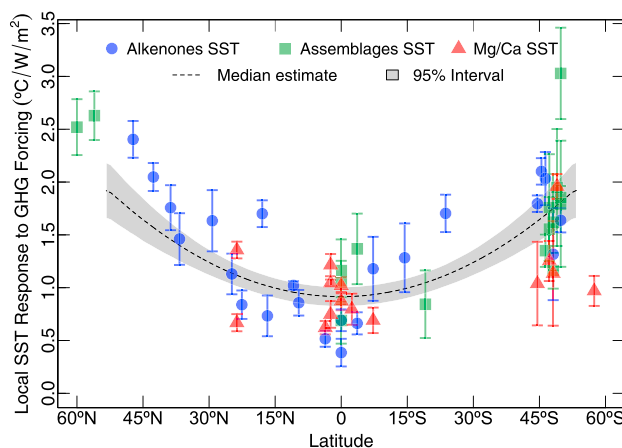


Figure 4. Latitudinal pattern of local SST response to changes in radiative forcing from GHGs. Each point represents the local SST responsiveness of one proxy reconstruction to climate change, represented here by deviations in GHG radiative forcing, as estimated from independent regressions (section 4.1). Colors indicate the temperature proxy method (alkenone indices in blue circles, Mg/Ca ratios in red triangles, and species assemblage methods in green squares). Error bars display 95% intervals. The equator-to-pole gradient of SST response is estimated from a regression of the 54 responsiveness values against $\sin^2(\text{latitude})$: the dashed line is the estimate, and the grey area is the 95% interval from the single regression.

include both the uncertainty within the SST reconstructions as well as the uncertainty in the estimate of local SST responsiveness from the previous regressions.

Another methodological alternative would be to implement a multivariate regression model where all the observations are modeled in a single model that includes independent variables for each of the reconstruction-specific variables, as well as the observation-specific variables. This method has the limitations of insufficient characterization for the uncertainty in the estimates, because the regression ignores that groups of observations come from the same reconstructions with correlated uncertainty. Additionally, interactive variables in this model cause multicollinearity and unstable results, as well as large reductions in degrees of freedom. Therefore, I develop a Bayesian hierarchical regression, which does not have these limitations, to assess the patterns of variation within and between SST reconstructions.

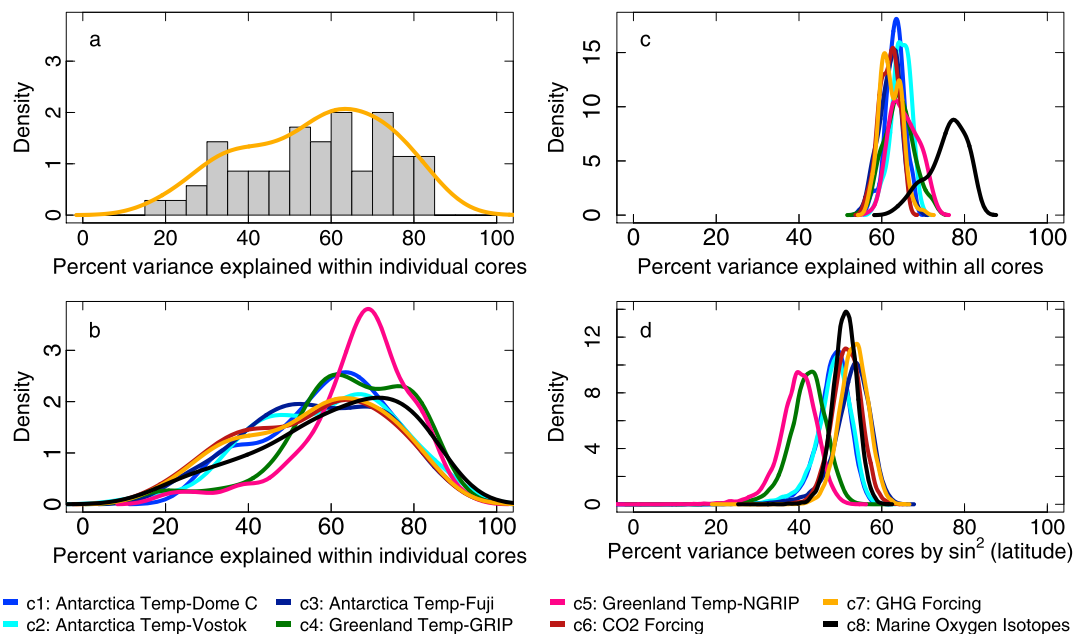


Figure 5. Percent variance explained within the SST reconstructions by the local SST responsiveness metric. (a) Histogram and empirically fit frequency distribution of the 54 adjusted R^2 values from the 54 independent regressions in Figure 4. (b) The same distributions as Figure 4a repeated for each of the eight climate indicators. Empirically fit frequency distributions of the adjusted R^2 values from the Bayesian hierarchical regressions of the 54 SST reconstructions for (c) the percent of total variance within all SST reconstructions explained by the eight climate indicators, adjusted R^2 values of the level one model from the bootstrap analysis and (d) the percent of total variance between all cores explained by $\sin^2(\text{latitude})$, adjusted R^2 values of the level two (hyperparameter) model. The eight different climate indicators are Antarctic temperature (c1 in blue, c2 in cyan, and c3 in navy), Greenland temperature (c4 in dark green and c5 in pink), GHG radiative forcing (c6 in orange and c7 in red), and bottom water oxygen-18 isotopes (c8 in black) (see section 2 and Table 1).

4.2. Bayesian Hierarchical (Multilevel) Regression Analysis

A hierarchical/multilevel model is a regression model where two or more linked regressions are estimated simultaneously; see *Gelman and Hill* [2007] for further details. Hierarchical models are able to simultaneously analyze patterns of commonality and variability within and between SST reconstructions. The hierarchical model is structured to match the grouping of the data in 54 SST reconstructions. One set of regressions explains the variation within each SST reconstruction (a “level one” model), such as the linear relationship of a single tropical SST reconstruction with changes in climate indicator like GHG forcing. Another set of regressions explains the variation between the different SST reconstructions (a “level two” model), such as the effect of latitude or proxy method on the estimates of local SST responsiveness of different SST reconstructions. The level two equation models how the regression parameters from the level one model vary between the SST reconstructions. The level one model is similar to equation (6), and the level two model is similar to equation (7) from section 4.1. The Bayesian hierarchical regression is a coupling of those two multivariate regressions, where the regression parameters for each core are sampled from a common distribution, defined by the level two model.

The critical difference with Bayesian hierarchical regressions as compared to the frequentist approach in section 4.1 is that Bayesian hierarchical regressions simultaneously estimate the two levels of regressions and optimize the sharing of information across SST reconstructions [*Gelman and Hill*, 2007]. Through optimal sharing of information, Bayesian hierarchical regressions enable significance tests of a larger variety of variables as compared to the methods discussed in section 4.1. Hierarchical models also enable the correct characterization of the structure of the regression error terms (covariance matrix for the residuals). For these reasons, the Bayesian hierarchical regression is the preferred method and the results of this paper focus on the hierarchical model results.

This research applies a weighted least squares model for the level one regression model within the Bayesian hierarchical regression using estimates of uncertainty in the SST proxy reconstructions. The level one model includes two types of independent variables: (1) the eight different records investigated separately as potential climate indicators, \mathbf{X} (matrix), and (2) variables that are thought to directly impact local SST change, \mathbf{X}^0 (matrix), such as time or glacial versus interglacial periods. The regression coefficients for the climate indicators, \mathbf{X} , are β_j (vector) and are the estimates of local SST responsiveness, and they are modeled in the level two regression model to estimate the effect of reconstruction-specific variables, \mathbf{U}_j (vector), such as proxy method, latitude, and ocean, on local SST responsiveness. The regression coefficients for \mathbf{U}_j are G (vector). The coefficients for \mathbf{X}^0 are β^0 (vector) and are not modeled in the level two regression model.

$$\text{Level one model : } \hat{y}_i \sim N \left(\mathbf{X}_i^0 \beta^0 + \mathbf{X}_i \beta_{j|t_i}, \hat{\sigma}_{y_i}^2 \right) \tag{8}$$

$$\text{Level two model : } \beta_j \sim N \left(\mathbf{U}_j G, \Sigma_B \right) \tag{9}$$

where i is the index over the 12,105 SST point reconstructions, j is the index over the 54 SST reconstructions, \hat{y}_i is the SST reconstruction j at time t_i (single value), $\hat{\sigma}_{y_i}^2$ is the variance for predicted y value at time t_i (single value), and Σ_B is the covariance matrix for the modeled coefficients. Residual analysis confirms that the model specification of equations (8) and (9) is appropriate. For example, for the model results in Figure 6, the level one residuals and level two residuals do behave as zero-mean white noise.

The core research presented here investigates the effect of latitude on local SST responsiveness. Such a model includes a single variable of $\sin^2(\text{latitude})$ in \mathbf{U}_j , which are core-specific variables thought to impact SST responsiveness. It does not include \mathbf{X}^0 variables, which are variables thought to directly impact local SST change. The results are shown in Figures 5c, 5d, and Table S3. The estimates calculated with the no pooling or “independent” regressions (Figure 4 and Table S1) are very similar to those estimated from the Bayesian hierarchical regressions (Figure 6 and Table S3), partially because there are a large number of observations in each SST record (over 200 on average).

I estimate posterior distributions by fitting the above Bayesian hierarchical regressions using Markov Chain Monte Carlo (MCMC) simulation and Gibbs sampling. I use an inverse Wishart model for the covariance matrix of the modeled coefficients, Σ_B [*Gelman and Hill*, 2007]. I implement this analysis using the program Just Another Gibbs Sampler (<http://www-fis.iarc.fr/~martyn/software/jags/>) via the “rjags” package in the R statistical program (<http://cran.r-project.org/web/packages/rjags/index.html>); see Text S2. I use the following priors

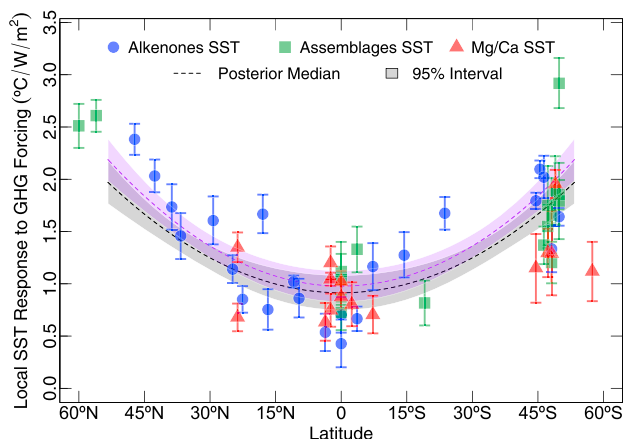


Figure 6. Latitudinal pattern of local SST response to changes in radiative forcing from GHGs. Each point represents the local SST responsiveness of one proxy reconstruction to climate change, represented here by deviations in GHG radiative forcing, as estimated from Bayesian hierarchical regressions (section 4.2). Colors and shapes as in Figure 4. Error bars display 95% intervals. The equator-to-pole gradient of SST response is estimated using a Bayesian hierarchical regression for $\sin^2(\text{latitude})$: the dashed line is the median estimate, and the grey area is the 95% interval from the MCMC simulation. An additional equator-to-pole gradient of SST response is estimated using a Bayesian hierarchical regression for the effect of $\sin^2(\text{latitude})$, the Indian Ocean, and the Mg/Ca proxy interactive with $\sin^2(\text{latitude})$ on local SST responsiveness: the purple dashed line is the median estimate, and the purple area is the 95% interval from the MCMC simulation.

with the climate indicator variable. For example, there may be trends in SST over time due to issues with the reconstruction or long-term cooling trends. Also, patterns of SST change may vary between interglacial and glacial periods or between different periods in time (such as 100 kyr periods). The following additional variables are evaluated in the level one model, \mathbf{X}^0 : time (continuous), time (discrete, in 100 kyr periods), and glacial versus interglacial periods (discrete indicator). All the variables in \mathbf{X}^0 are tested directly and in interaction with the climate indicator. Estimates of the dates of the last five interglacial periods (last 450 kyr) are taken from a combination of resources [Sirocko et al., 2007; Jouzel et al., 2007; Jansen et al., 2007] to be 0–16 kyr, 114–133 kyr, 236–245 kyr, 321–338 kyr, and 395–427 kyr. All the level one variables (\mathbf{X}^0) are found to not be significant across all eight climate indicators in directly changing SST response and in interaction with the climate indicator (their estimated coefficients are not significantly different from zero at the 95% confidence level).

There are some core-specific variables that might impact the responsiveness of SST. For example, locations at higher latitudes are likely to show greater changes in SST per a given climate change. However, the exact functional relationship for patterns of SST responsiveness with latitude is debated in the literature [Hoffert and Covey, 1992; Covey et al., 1996; Shabalova and Können, 1995; Zachos et al., 1994], and thus, several functional forms are tested here. In addition, the absolute SST of the core may influence its responsiveness as may the ocean basin or the proxy method. The following additional reconstruction-specific variables are modeled in the level two model, \mathbf{U}_j : proxy method, ocean basin, SST reconstruction length (in time), SST reconstruction average resolution, SST reconstruction average temperature (over full core, 0–12 kyr, 30–90 kyr, and 0–100 kyr), functions of latitude (latitude, latitude², latitude³, latitude⁴, sin(latitude), sin²(latitude), sin³(latitude), sin⁴(latitude)), and functions of longitude (longitude, cos(longitude)), interactions of sin²(latitude) with proxy, and interactions of sin²(latitude) with ocean. For ocean basin definitions, I use boundaries from the current convention (International Hydrographic Bureau 1953) [MARGO Project Members, 2009]: 20°E as the boundary between the Atlantic and Indian Oceans, 147°E as the boundary between the Indian and Pacific Oceans, and 68°W as the boundary between the Pacific and Indian Oceans. I do not distinguish the Nordic Seas, Arctic Ocean, and Southern Ocean. The only level two, reconstruction-specific variables (\mathbf{U}_j) found to be significant in changing local SST responsiveness across all eight climate indicators

for the regression coefficients and variances: uniform distribution (0,100) for σ_y and normal distribution (mean = 0, standard deviation = 100) for all regression coefficients (β^0, G), as specified by Gelman and Hill [2007]. I estimate a Bayesian R^2 for the level two model that is analogous to the classical adjusted R^2 using the method from Gelman and Hill [2007], which produces a conservative estimate.

I simulate the final models for 25,000 iterations, discard 5000 iterations as burn in, and thin by one fourth. I run all models for four independent chains, with random initial values selected from the priors. I confirm convergence by finding that the Potential Scale Reduction Factor \hat{R} diagnostic [Gelman and Rubin, 1992] is roughly equal to 1 for all model parameters using the “ggmcmc” package in the R statistical program (<https://cran.r-project.org/web/packages/ggmcmc/index.html>).

There are some core-specific variables that might directly impact local SST change, either directly or in interaction

(their estimated coefficients are significantly different from zero at the 95% confidence level) are the Indian Ocean and the Mg/Ca proxy in interaction with $\sin^2(\text{latitude})$.

There is also uncertainty introduced from the particular set of 54 SST reconstructions, which are limited in their spatial coverage and their temporal resolution. The nonrandom and limited samples make generalizations from specific proxy records uncertain. *Moss and Schneider* [2000] emphasize the need to quantify such structural uncertainty. I test the sensitivity of the Bayesian regressions results to particular SST reconstructions through 100 simulations of random resampling with replacement of the 54 SST reconstructions, repeated for each of the eight climate indicators, and then rerun the Bayesian regressions. The variation in results from such a bootstrap analysis reflects the uncertainty introduced from the specific sample of records. The Bayesian regressions adequately estimate uncertainty in model coefficients but underestimate uncertainty in adjusted R^2 values for the level one models. I summarize results across all eight climate indicators as follows: equal weighting to the ensemble of Antarctic temperature records, to the ensemble of Greenland temperature records, to the pair of GHG forcing reconstructions, and to the deep-sea oxygen isotope reconstruction. In addition to resampling the 54 SST reconstructions, I test sensitivity to time by running 10 independent analyses covering varying 100 kyr periods for each of the eight climate indicators. Time is also tested as an independent variable in multiple forms in the level one model (see previous section on \mathbf{X}^0 components).

5. Results and Discussion

5.1. Local SST Responsiveness

This research examines the pattern of local SST response to climate change by regressing the 54 SST reconstructions as a function of eight different climate indicators. Figure 3 illustrates example regression plots for individual SST reconstructions. Figure 4 shows estimates of the local SST response relative to changes in GHG radiative forcing for all 54 SST reconstructions from independent regressions (section 4.1). Figure 5a shows the associated percent of variance explained within each SST reconstruction by the climate indicator (estimated adjusted R^2). The same analysis is repeated for all eight climate indicators, and the adjusted R^2 values are summarized in Figure 5b. The local SST responsiveness estimates from the Bayesian hierarchical regression (section 4.2 and Figure 6) are similar to the independent regressions (Figure 4) due to the large sample size. However, there are some important differences between the results of Figures 4 and 6. Some outlier cores are pulled closer to the expected median of the hierarchical regression with reduced uncertainty estimates. There also are important differences in the estimated latitudinal gradients of SST responsiveness (see section 5.2).

The adjusted R^2 estimates from the level one Bayesian hierarchical regressions displayed in Figure 5c represent the percent variation explained within all reconstructions by a single responsiveness variable for each SST reconstruction. The percent of variance explained within each SST reconstruction when considered individually (Figure 5b) has greater uncertainty than when considered together in a multilevel model (Figure 5c), as would be expected. A single local responsiveness estimate for each SST reconstruction combined with a climate indicator record is able to explain 64% (58% to 81%, 95% interval from the bootstrap analysis) of the variation among all the 12,105 local SST estimates that span the last million years (Figure 5c). The deep-sea oxygen isotope record has the greatest explanatory power for changes in local SST, but that is perhaps because of the use of the oxygen isotope record in the dating of SST reconstructions.

The predictive capacity of local temperature response is stable over time and over random resampling of the SST records, as tested by comparing the coefficient and adjusted R^2 estimates from the level one Bayesian hierarchical regressions across 100 kyr increments and across the bootstrap resampling of the 54 ocean cores. These results suggest that there is a stable, linear relationship between local SST response and climate changes over the past million years. Moreover, the concept of a stable value of local SST responsiveness is robust across eight different climate indicators. This new variable of local SST responsiveness could be used in other analyses as a coarse summary statistic for the behavior of different SST reconstructions, because it captures over 60% of variation within the SST reconstructions.

5.2. Latitude

As is apparent in Figure 6, the estimates of local SST responsiveness display an expected pattern of the high latitudes changing more than the tropics [*Hoffert and Covey*, 1992; *Covey et al.*, 1996; *Shabalova and Können*, 1995; *Zachos et al.*, 1994]. One metric to summarize the relative amplification of SST change with latitude or the tropical attenuation of SST is to estimate the zonal (by latitude) mean temperature change relative to

a specific global mean temperature change. *Hoffert and Covey* [1992] estimated latitudinal curves of zonal mean temperature change relative to global mean temperature change for three different time points. They found the same curve that described all three time points, despite dramatically different climate conditions. *Hoffert and Covey* [1992] suggested that such a relationship might be a “universal curve” of the zonal temperature change per global temperature change. Since their analysis, many proxy errors have been corrected and more proxy data have become available, especially from ocean cores [*Mix et al.*, 2001]. This research uses an extensive database of over 12,000 SST proxy reconstructions over the past 400 kyr to test the concept of a universal curve of SST response. The latitude results are limited to the past 400 kyr due to the availability of high-latitude SST reconstructions.

Change in SST relative to change in climate indicators as a function of $\sin^2(\text{latitude})$ (Figure 6 and Table S3) explains 50% (35% to 58%, 95% interval) of the observed variance in responsiveness between ocean cores, as estimated by adjusted R^2 estimates from the level two Bayesian hierarchical regressions (Figure 5d). Thus, latitude alone can account for half of the differences observed between SST reconstructions from across the globe, regardless of SST proxy, ocean basin, or time period. Over the past 400 kyr, SST change at 45°N/S is larger than the average tropical response by a factor of 1.9 (1.5 to 2.6, 95% interval) (Table S3).

The estimated latitudinal curve from the hierarchical model (Figure 6) is similar to the curve estimated from the independent regressions (Figure 4) but has several key differences. The estimate of uncertainty is larger at the tropical latitudes in the hierarchical model because of the model's more robust analysis of uncertainty. I define a summary metric for the latitudinal curves that pools results across the eight climate indicators (see section 4.2 for weighting of the climate indicators): the ratio of SST change at 45°N/S compared to tropical SST change. The hierarchical regression model estimates a summary metric of 1.9 (1.5 to 2.6, 95% interval), while the independent regression method estimates a similar summary metric of 2.0 (1.7 to 2.2, 95% interval) but with insufficient uncertainty estimation. When proxy and ocean variables are included in the level two model (see sections 5.3 and 5.4), the estimated latitudinal curve from the hierarchical model exhibits the following critical changes (Figure 6): the tropical response increases due to the estimate of decreased responsiveness in the Indian Ocean (section 5.3), and the latitudinal gradient is steeper due to the estimate of attenuation of SST responsiveness with latitude in Mg/Ca ratio-based SST reconstructions (section 5.4). The updated summary metric is still similar because the two effects roughly cancel each other out at 45°N/S: 2.0 (1.5 to 2.6, 95% interval).

Previous research on latitudinal gradients focused on absolute temperature gradients and modeled temperature as a function of $\sin(\text{latitude})$ to the third [*Zachos et al.*, 1994] or fourth power [*Hoffert and Covey*, 1992; *Covey et al.*, 1996; *Shabalova and Können*, 1995]. This analysis, however, finds the best fit for a function of $\sin^2(\text{latitude})$ and finds no significant improvement in fit for other powers of latitude beyond a quadratic term, with fit assessed from the adjusted R^2 estimates from the level two Bayesian hierarchical regressions. The difference in latitude functions could be because others analyzed air surface temperature over the full latitude range, whereas this research focuses on SST over 50°N–50°S. The different functional estimates could also be due to improved SST proxy records, especially in the tropics. *Rohling et al.* [2012] also found a quadratic fit for the latitudinal pattern of mean long-term linear temperature response from independent regressions of 36 SST reconstructions compared to a reconstruction global mean radiative forcing. *Rohling et al.* [2012] also expanded their analysis to compare latitudinal patterns of SST to latitudinal patterns for changes in radiative forcing. It is important to note that the symmetric latitudinal curve is a coarse approximation of the observed pattern of SST responsiveness, and that more data would likely demonstrate asymmetry across the hemispheres due to the unequal distribution of landmasses and varying ocean currents and the curve would not necessarily be centered exactly at the equator.

Note that the estimated SST latitudinal response curves are limited to 50°N–50°S, because latitudes above 50°N/S have a muted response to climate changes due to freezing and sea ice dynamics. There are insufficient records available for high latitudes to estimate a functional relationship for this muted response. However, it is worth noting that the zone of 50°N to 50°S still contains 77% of the Earth's surface. In addition, the data are insufficient to estimate significant differences between the Northern and Southern Hemispheres. The estimates also are limited by the sparse availability of SST reconstructions from the North Pacific Ocean.

The estimated SST response curve is robust to a variety of sensitivity tests, suggesting that the curve is perhaps generally “universal” [*Hoffert and Covey*, 1992] over the past 400 kyr. The SST response curve does not vary significantly when tested independently over 100 kyr periods, between glacial and interglacial periods,

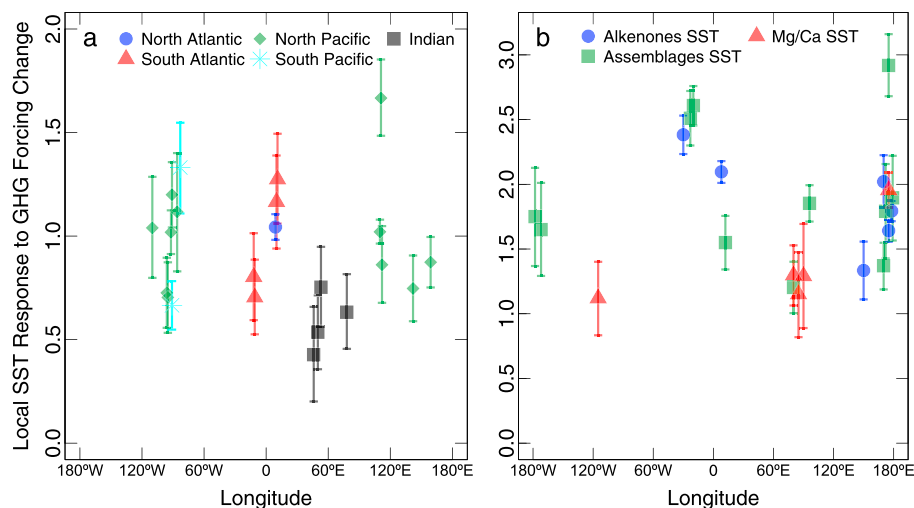


Figure 7. Local SST responsiveness to changes in GHG radiative forcing differentiated by ocean at low latitudes and by proxy at high latitudes. Longitudinal cross section of local SST response to GHG radiative forcing is displayed for tropical latitudes (15°N–15°S) and high latitudes (40°–60°N/S). (a) Shapes and colors indicate the ocean basin: North Atlantic in blue circles, South Atlantic in red triangles, North Pacific in green diamonds, South Pacific in cyan asterisks, and Indian in black squares. (b) Shapes and colors indicate the temperature proxy method as in Figure 4. Error bars are 95% intervals.

and during glacial terminations. The SST response curve also does not vary significantly with random resampling of the cores or across the eight climate indicators, suggesting that the results are not contingent to this specific combination of reconstructions. Local absolute SST does not significantly affect the average SST change in response to climate indicators, once latitude is modeled.

5.3. Oceans

The only ocean variable with a coefficient significantly different from zero at the 95% confidence level is the Indian Ocean. Tropical SST reconstructions from the Indian Ocean have a weaker local SST response to climate changes than predicted by latitude alone for all eight climate indicators. The Indian Ocean displays a reduction in response in tropical SST change of 50% (12% to 95%, 95% interval) less than that found at similar latitudes in other oceans (Figure 7a). A literature search did not find discussions of a systematic muted response of SST reconstructions in the Indian Ocean relative to other oceans. One of the ways the Indian Ocean differs from the Atlantic and Pacific Oceans is that it “is bounded to the north by the Asian continent, preventing northward heat export and only allowing weak ventilation of the Indian Ocean thermocline from the north” [Schott *et al.*, 2009]. Perhaps that difference in flow causes a modulation of the SST responsiveness of the Indian Ocean, despite communication with the Pacific Ocean through the Indonesian Throughflow. In addition, other research has found that global climate changes likely cause changes in the Indian Ocean Dipole [Cai *et al.*, 2013; Shukla *et al.*, 2009]. Changes in the Indian Ocean Dipole may be driving the different SST responsiveness observed in the Indian Ocean relative to other oceans.

5.4. Proxies

There is significant agreement among the different updated proxy SST reconstructions: coefficients for proxy variables are not significantly different from zero at the 95% confidence level except for the interactive term between Mg/Ca proxy and $\sin^2(\text{latitude})$. This result confirms recent claims that progress in SST proxy methods has successfully reduced many of the systematic biases found in previous reconstructions (see section 2). These results extend previous multiproxy comparisons over continuous time and multiple reconstructions in a single analysis and confirm significant progress in the proxy methods. When more than one SST reconstruction is available from species abundance methods, I analyze separately the different analytical methods and warm/cold season outputs and find that the local temperature response estimates are not significantly different from each other. Therefore, I use a single-average result with a variance representing the different estimates for each reconstruction using species abundance methods. The Mg/Ca ratio-based SST reconstructions estimate significantly smaller SST response at higher latitudes, a reduction of 35% (7% to 59%, 95% interval) at 45°N/S compared to the magnitude of other proxy methods at similar latitudes (Figure 7b).

Other studies also have found significant deviation in Mg/Ca SST reconstructions from other proxy reconstructions at high latitudes, including a tendency to underpredict SST variations [Kandiano *et al.*, 2004; Barker *et al.*, 2005; Meland *et al.*, 2005].

6. Conclusions

This research adds to our understanding of the response of SST to climate changes. It finds that a new summary statistic of local SST responsiveness is able to explain over 60% of the variation within SST reconstructions with only a single value per SST reconstruction. Moreover, the relationship between local SST response and climate change over the past million years is linear and stable over time. The results are not sensitive to the particular climate indicator chosen: eight climate indicators were evaluated.

This study finds evidence for a universal curve of local SST response as a function of latitude that is stable over the past 400 kyr. The existence of such a universal curve advances our knowledge of how the climate responds spatially to large changes in radiative forcing and provides important insights into the mechanisms of key climate dynamics, such as polar amplification. This research also explores variation across SST proxy methods. It finds remarkable agreement across proxy methods, with the exception of Mg/Ca proxy methods estimating muted responses at high latitudes. The Indian Ocean also exhibits a muted temperature response in comparison to other oceans.

This research illustrates the diversity of questions that can be tested by applying probabilistic analysis and Bayesian hierarchical regressions to the study of past climate variables. These methods enable paleoclimatologists to investigate a greater number of variables and relationships with more explicit uncertainty estimates. Moreover, this research develops a new method for incorporating consideration of uncertain timescales into record intercomparisons. These uncertainty and statistical methods are well suited for application across paleoclimate and environmental data series intercomparisons.

Acknowledgments

Richard Samworth (University of Cambridge) was instrumental in developing the dating uncertainty method. I thank C. Warsaw, S. Schneider, C. Tebaldi, R. Dunbar, K. Caldeira, C. Field, H. Elderfield, and two anonymous reviewers for advice and feedback. This research is indebted to many scientists for supplying their proxy data records (see Table 1) and to NOAA's National Centers for Environmental Information and PANGAEA. The data reported in this paper are archived in Data Set S1. This study was supported by the National Science Foundation Graduate Research Fellowship and the Marshall Scholarship. The views expressed in this article are those of the author and do not necessarily reflect the views or policies of the U.S. Environmental Protection Agency.

References

- Anand, P., H. Elderfield, and M. H. Conte (2003), Calibration of Mg/Ca thermometry in planktonic foraminifera from a sediment trap time series, *Paleoceanography*, *18*(2), 1050, doi:10.1029/2002PA000846.
- Bard, E. (2001), Comparison of alkenone estimates with other paleotemperature proxies, *Geochemistry Geophysics Geosystems*, *2*, 1002, doi:10.1029/2000GC000050.
- Bard, E. (2002), Climate shock—Abrupt changes over millennial time scales, *Phys. Today*, *55*(12), 32–38.
- Bard, E., F. Rostek, and C. Sonzogni (1997), Interhemispheric synchrony of the last deglaciation inferred from alkenone palaeothermometry, *Nature*, *385*(6618), 707–710.
- Barker, S., M. Greaves, and H. Elderfield (2003), A study of cleaning procedures used for foraminiferal Mg/Ca paleothermometry, *Geochem. Geophys. Geosyst.*, *4*, 8407, doi:10.1029/2003GC000559.
- Barker, S., I. Cacho, H. Benway, and K. Tachikawa (2005), Planktonic foraminiferal Mg/Ca as a proxy for past oceanic temperatures: A methodological overview and data compilation for the Last Glacial Maximum, *Quat. Sci. Rev.*, *24*(7/9), 821–834.
- Barrows, T. T., S. Juggins, P. De Deckker, E. Calvo, and C. Pelejero (2007), Long-term sea surface temperature and climate change in the Australian-New Zealand region, *Paleoceanography*, *22*, PA2215, doi:10.1029/2006PA001328.
- Birks, H. J. B., O. Heiri, H. Seppä, and A. E. Bjune (2010), Strengths and weaknesses of quantitative climate reconstructions based on Late-Quaternary, *Open Ecol. J.*, *3*(1), 68–110.
- Brathauer, U., and A. Abelmann (1999), Late Quaternary variations in sea surface temperatures and their relationship to orbital forcing recorded in the Southern Ocean (Atlantic sector), *Paleoceanography*, *14*(2), 135–148.
- Breitenbach, S., et al. (2012), Constructing proxy records from age models (COPRA), *Clim. Past*, *8*(5), 1765–1779.
- Brown, S. J., and H. Elderfield (1996), Variations in Mg/Ca and Sr/Ca ratios of planktonic foraminifera caused by postdepositional dissolution: Evidence of shallow Mg-dependent dissolution, *Paleoceanography*, *11*(5), 543–551.
- Cai, W., X.-T. Zheng, E. Weller, M. Collins, T. Cowan, M. Lengaigne, W. Yu, and T. Yamagata (2013), Projected response of the Indian Ocean dipole to greenhouse warming, *Nat. Geosci.*, *6*(12), 999–1007.
- Clark, J. S., and A. E. Gelfand (2006), *Hierarchical Modelling for the Environmental Sciences: Statistical Methods and Applications*, 205 pp., Oxford Univ. Press, New York.
- Clemens, S. C., W. L. Prell, Y. Sun, Z. Liu, and G. Chen (2008), Southern Hemisphere forcing of Pliocene $\delta^{18}O$ and the evolution of Indo-Asian monsoons, *Paleoceanography*, *23*, PA4210, doi:10.1029/2008PA001638.
- Climate: Long-Range Investigation, Mapping, and Prediction (CLIMAP) Project Members (1981), Seasonal reconstruction of the earth's surface at the last glacial maximum, *Map and Chart Ser.*, *36*, Geol. Soc. of Am., Boulder, Colo.
- Covey, C., L. C. Sloan, and M. I. Hoffert (1996), Paleoclimate data constraints on climate sensitivity: The paleocalibration method, *Clim. Change*, *32*(2), 165–184.
- Cuffey, K. M., and F. Vimeux (2001), Covariation of carbon dioxide and temperature from the Vostok ice core after deuterium-excess correction, *Nature*, *412*(6846), 523–527.
- de Garidel-Thoron, T., Y. Rosenthal, F. Bassinot, and L. Beaufort (2005), Stable sea surface temperatures in the western Pacific warm pool over the past 1.75 million years, *Nature*, *433*(7023), 294–298.
- Eglinton, G., S. A. Bradshaw, A. Rosell, M. Sarnthein, U. Pflaumann, and R. Tiedemann (1992), Molecular record of secular sea surface temperature changes on 100-year timescales for glacial terminations I, II and IV, *Nature*, *356*(6368), 423–426.
- Elderfield, H., and G. Ganssen (2000), Past temperature and delta O-18 of surface ocean waters inferred from foraminiferal Mg/Ca ratios, *Nature*, *405*(6785), 442–445.

- Fan, J., and Q. Yao (1998), Efficient estimation of conditional variance functions in stochastic regression, *Biometrika*, 85(3), 645–660.
- Gelman, A., and J. Hill (2007), *Data Analysis Using Regression and Multilevel/Hierarchical Models, Analytical Methods for Social Research*, Cambridge Univ. Press, Cambridge, U. K., and New York.
- Gelman, A., and D. B. Rubin (1992), Inference from iterative simulation using multiple sequences, *Statist. Sci.*, 7(4), 457–472.
- Genthon, C., J. M. Barnola, D. Raynaud, C. Lorius, J. Jouzel, N. I. Barkov, Y. S. Korotkevich, and V. M. Kotlyakov (1987), Vostok ice core: Climatic response to CO₂ and orbital forcing changes over the last climatic cycle, *Nature*, 329(6138), 414–418.
- Gonzalez, E. L., U. Riebesell, J. M. Hayes, and E. A. Laws (2001), Effects of biosynthesis and physiology on relative abundances and isotopic compositions of alkenones, *Geochem. Geophys. Geosyst.*, 2, 1004, doi:10.1029/2000GC000052.
- Haam, E., and P. Huybers (2010), A test for the presence of covariance between time-uncertain series of data with application to the Dongge Cave speleothem and atmospheric radiocarbon records, *Paleoceanography*, 25, PA2209, doi:10.1029/2008PA001713.
- Hansen, J., M. Sato, P. Kharecha, D. Beerling, R. Berner, V. Masson-Delmotte, M. Pagani, M. Raymo, D. L. Royer, and J. C. Zachos (2008), Target atmospheric CO₂: Where should humanity aim?, *Open Atmos. Sci. J.*, 2(1), 217–231.
- Haslett, J., M. Whitley, S. Bhattacharya, M. Salter-Townshend, S. P. Wilson, J. R. M. Allen, B. Huntley, and F. J. G. Mitchell (2006), Bayesian palaeoclimate reconstruction, *J. R. Stat. Soc. A*, 169(3), 395–438.
- Herbert, T. D. (2001), Review of alkenone calibrations (culture, water column, and sediments), *Geochem. Geophys. Geosyst.*, 2, 1055, doi:10.1029/2000GC000055.
- Hoffert, M. I., and C. Covey (1992), Deriving global climate sensitivity from palaeoclimate reconstructions, *Nature*, 360(6404), 573–576.
- Horikawa, K., M. Minagawa, M. Murayama, Y. Kato, and H. Asahi (2006), Spatial and temporal sea-surface temperatures in the eastern equatorial Pacific over the past 150 kyr, *Geophys. Res. Lett.*, 33, L13605, doi:10.1029/2006GL025948.
- Huybers, P. (2007), Glacial variability over the last two million years: An extended depth-derived age model, continuous obliquity pacing, and the Pleistocene progression, *Quat. Sci. Rev.*, 26(1–2), 37–55.
- Huybers, P., and C. Wunsch (2004), A depth-derived Pleistocene age model: Uncertainty estimates, sedimentation variability, and nonlinear climate change, *Paleoceanography*, 19, PA1028, doi:10.1029/2002PA000857.
- Jansen, E., et al. (2007), *Palaeoclimate, Book Section 6*, pp. 433–497, Cambridge Univ. Press, Cambridge, U. K.
- Jones, P., et al. (2009), High-resolution palaeoclimatology of the last millennium: A review of current status and future prospects, *Holocene*, 19(1), 3–49.
- Jouzel, J., et al. (2007), Orbital and millennial Antarctic climate variability over the past 800,000 years, *Science*, 317(5839), 793–796, doi:10.1126/science.1141038.
- Kandiano, E. S., H. A. Bauch, and A. Muller (2004), Sea surface temperature variability in the North Atlantic during the last two glacial-interglacial cycles: Comparison of faunal, oxygen isotopic, and Mg/Ca-derived records, *Palaeogeogr. Palaeoclimatol. Palaeoecol.*, 204(1–2), 145–164.
- Kawamura, K., et al. (2007), Northern Hemisphere forcing of climatic cycles in Antarctica over the past 360,000 years, *Nature*, 448(7156), 912–916.
- Kheshgi, H. S., and A. G. Lapeis (1996), Estimating the uncertainty of zonal paleotemperature averages, *Palaeogeogr. Palaeoclimatol. Palaeoecol.*, 121, 221–237.
- Kucera, M., A. Rosell-Mele, R. Schneider, C. Waelbroeck, and M. Weinelt (2005a), Multiproxy Approach for the Reconstruction of the Glacial Ocean Surface (MARGO), *Quat. Sci. Rev.*, 24(7/9), 813–819.
- Kucera, M., M. Weinelt, T. Kiefer, U. Pflaumann, A. Hayes, M. Weinelt, M. T. Chen, A. C. Mix, T. T. Barrows, and E. Cortijo (2005b), Reconstruction of sea-surface temperatures from assemblages of planktonic foraminifera: Multi-technique approach based on geographically constrained calibration data sets and its application to glacial Atlantic and Pacific Oceans, *Quat. Sci. Rev.*, 24(7–9), 951–998.
- Labeyrie, L., et al. (1996), Hydrographic changes of the Southern Ocean (southeast Indian Sector) over the last 230 kyr, *Paleoceanography*, 11(1), 57–76.
- Lawrence, K. T., Z. H. Liu, and T. D. Herbert (2006), Evolution of the eastern tropical Pacific through Plio-Pleistocene glaciation, *Science*, 312(5770), 79–83.
- Lea, D. W. (2004), The 100,000-yr cycle in tropical SST, greenhouse forcing, and climate sensitivity, *J. Clim.*, 17(11), 2170–2179.
- Lea, D. W., T. A. Mashiotta, and H. J. Spero (1999), Controls on magnesium and strontium uptake in planktonic foraminifera determined by live culturing, *Geochim. Cosmochim. Acta*, 63(16), 2369–2379.
- Lea, D. W., D. K. Pak, and G. Paradis (2005), Influence of volcanic shards on foraminiferal Mg/Ca in a core from the Galápagos region, *Geochem. Geophys. Geosyst.*, 6, Q11P04, doi:10.1029/2005GC000970.
- Lea, D. W., D. K. Pak, C. L. Belanger, H. J. Spero, M. A. Hall, and N. J. Shackleton (2006), Paleoclimate history of Galapagos surface waters over the last 135,000yr, *Quat. Sci. Rev.*, 25(11/12), 1152–1167.
- Li, B., D. W. Nychka, and C. M. Ammann (2007), The hockey stick and the 1990s: A statistical perspective on reconstructing hemispheric temperatures, *Tellus A*, 59(5), 591–598.
- Li, B., D. W. Nychka, and C. M. Ammann (2010a), The value of multiproxy reconstruction of past climate, *J. Am. Stat. Assoc.*, 105(491), 883–895.
- Li, B., D. W. Nychka, and C. M. Ammann (2010b), The value of multiproxy reconstruction of past climate, *J. Am. Stat. Assoc.*, 105(491), 883–895.
- Lin, L., D. Khider, L. E. Lisiecki, and C. E. Lawrence (2014), Probabilistic sequence alignment of stratigraphic records, *Paleoceanography*, 29(10), 976–989, doi:10.1002/2014PA002713.
- Lisiecki, L. E., and M. E. Raymo (2005), A Pliocene-Pleistocene stack of 57 globally distributed benthic delta O-18 records, *Paleoceanography*, 20, PA1003, doi:10.1029/2004PA001071.
- Lorius, C., J. Jouzel, D. Raynaud, J. Hansen, and H. Letreut (1990), The ice-core record: Climate sensitivity and future greenhouse warming, *Nature*, 347(6289), 139–145.
- Loulergue, L., A. Schilt, R. Spahni, V. Masson-Delmotte, T. Blunier, B. Lemieux, J. M. Barnola, D. Raynaud, T. F. Stocker, and J. Chappellaz (2008), Orbital and millennial-scale features of atmospheric CH₄ over the past 800,000 years, *Nature*, 453(7193), 383–386, doi:10.1038/nature06950.
- Lüthi, D., et al. (2008), High-resolution carbon dioxide concentration record 650,000–800,000 years before present, *Nature*, 453(7193), 379–382, doi:10.1038/nature06949.
- Multiproxy approach for the reconstruction of the glacial ocean surface (MARGO) Project Members (2009), Constraints on the magnitude and patterns of ocean cooling at the Last Glacial Maximum, *Nat. Geosci.*, 2(2), 127–132.
- Martinson, D. G., N. G. Pisias, J. D. Hays, J. Imbrie, T. C. Moore, and N. J. Shackleton (1987), Age dating and the orbital theory of the ice ages: Development of a high-resolution 0 to 300,000-year chronostratigraphy, *Quat. Res.*, 27(1), 1–29.

- Mashiotta, T. A., D. W. Lea, and H. J. Spero (1999), Glacial-interglacial changes in subantarctic sea surface temperature and delta O-18-water using foraminiferal Mg, *Earth Planet. Sci. Lett.*, 170(4), 417–432.
- Masson-Delmotte, V., J. Jouzel, A. Landais, M. Stievenard, S. J. Johnsen, J. W. C. White, M. Werner, A. Sveinbjornsdottir, and K. Fuhrer (2005), Atmospheric science: GRIP deuterium excess reveals rapid and orbital-scale changes in Greenland moisture origin, *Science*, 309(5731), 118–121.
- Masson-Delmotte, V., et al. (2006), Past temperature reconstructions from deep ice cores: Relevance for future climate change, *Clim. Past*, 2(2), 145–165.
- Medina-Elizalde, M., and D. W. Lea (2005), The mid-Pleistocene transition in the tropical Pacific, *Science*, 310(5750), 1009–1012.
- Meland, M. Y., E. Jansen, and H. Elderfield (2005), Constraints on SST estimates for the northern North Atlantic/Nordic Seas during the LGM, *Quat. Sci. Rev.*, 24(7/9), 835–852.
- Mix, A. C., E. Bard, and R. Schneider (2001), Environmental processes of the ice age: Land, oceans, glaciers (EPILOG), *Quat. Sci. Rev.*, 20(4), 627–657.
- Moss, R. H., and S. H. Schneider (2000), *Uncertainties in the IPCC TAR: Recommendations to Lead Authors for More Consistent Assessment and Reporting*, pp. 33–51, Intergovernmental Panel on Climate Change, Geneva, Switzerland.
- Müller, P. J., M. Cepek, G. Ruhland, and R. R. Schneider (1997), Alkenone and coccolithophorid species changes in late Quaternary sediments from the Walvis Ridge: Implications for the alkenone paleotemperature method, *Palaeogeogr. Palaeoclimatol. Palaeoecol.*, 135(1–4), 71–96.
- Müller, P. J., G. Kirst, G. Ruhland, I. Von Storch, and A. Rosell-Melé (1998), Calibration of the alkenone paleotemperature index U_{37}^k based on core-tops from the eastern South Atlantic and the global ocean (60°N–60°S), *Geochim. Cosmochim. Acta*, 62(10), 1757–1772.
- Nürnberg, D., A. Müller, and R. R. Schneider (2000), Paleo-sea surface temperature calculations in the equatorial east Atlantic from Mg/Ca ratios in planktic foraminifera: A comparison to sea surface temperature estimates from U_{37}^k , oxygen isotopes, and foraminiferal transfer function, *Paleoceanography*, 15(1), 124–134.
- Oppo, D. W., and Y. B. Sun (2005), Amplitude and timing of sea-surface temperature change in the northern South China Sea: Dynamic link to the East Asian monsoon, *Geology*, 33(10), 785–788.
- Pahnke, K., and J. P. Sachs (2006), Sea surface temperatures of southern midlatitudes 0–160 kyr BP, *Paleoceanography*, 21, PA2003, doi:10.1029/2005PA001191.
- Pahnke, K., R. Zahn, H. Elderfield, and M. Schulz (2003), 340,000-year centennial-scale marine record of Southern Hemisphere climatic oscillation, *Science*, 301(5635), 948–952.
- Pelejero, C., J. O. Grimalt, S. Heilig, M. Kienast, and L. J. Wang (1999), High-resolution U-37(K) temperature reconstructions in the South China Sea over the past 220 kyr, *Paleoceanography*, 14(2), 224–231.
- Pelejero, C., E. Calvo, T. T. Barrows, G. A. Logan, and P. De Deckker (2006), South Tasman Sea alkenone palaeothermometry over the last four glacial/interglacial cycles, *Mar. Geol.*, 230(1–2), 73–86.
- Pisias, N. G., and A. C. Mix (1997), Spatial and temporal oceanographic variability of the eastern equatorial Pacific during the Late Pleistocene: Evidence from radiolaria microfossils, *Paleoceanography*, 12(3), 381–393.
- Regenberg, M., S. Steph, D. Nürnberg, R. Tiedemann, and D. Garbe-Schönberg (2009), Calibrating Mg/Ca ratios of multiple planktonic foraminiferal species with δ 18 o-calcification temperatures: Paleothermometry for the upper water column, *Earth Planet. Sci. Lett.*, 278(3), 324–336.
- Rehfeld, K., N. Marwan, J. Heitzig, and J. Kurths (2011), Comparison of correlation analysis techniques for irregularly sampled time series, *Nonlinear Process. Geophys.*, 18(3), 389–404.
- Rickaby, R. E. M., and H. Elderfield (1999), Planktonic foraminiferal Cd/Ca: Paleonutrients or paleotemperature?, *Paleoceanography*, 14(3), 293–303.
- Robinson, M. M., H. J. Dowsett, G. S. Dwyer, and K. T. Lawrence (2008), Reevaluation of mid-Pliocene North Atlantic sea surface temperatures, *Paleoceanography*, 23, PA3213, doi:10.1029/2008PA001608.
- Rohling, E., M. Medina-Elizalde, J. Shepherd, M. Siddall, and J. Stanford (2012), Sea surface and high-latitude temperature sensitivity to radiative forcing of climate over several glacial cycles, *J. Clim.*, 25(5), 1635–1656.
- Rostek, F., E. Bard, L. Beaufort, C. Sonzogni, and G. Ganssen (1997), Sea surface temperature and productivity records for the past 240 kyr in the Arabian Sea, *Deep Sea Res. Part II*, 44(6/7), 1461–1480.
- Sachs, J. P., and R. F. Anderson (2003), Fidelity of alkenone paleotemperatures in southern Cape Basin sediment drifts, *Paleoceanography*, 18(4), 1082, doi:10.1029/2002PA000862.
- Saraswat, R., R. Nigam, S. Weldeab, A. Mackensen, and P. D. Naidu (2005), A first look at past sea surface temperatures in the equatorial Indian Ocean from Mg/Ca in foraminifera, *Geophys. Res. Lett.*, 32, L24605, doi:10.1029/2005GL024093.
- Schneider, R. R., P. J. Müller, and G. Ruhland (1995), Late Quaternary surface circulation in the east equatorial South Atlantic: Evidence from alkenone sea surface temperatures, *Paleoceanography*, 10(2), 197–219.
- Schott, F. A., S.-P. Xie, and J. P. McCreary (2009), Indian ocean circulation and climate variability, *Rev. Geophys.*, 47, RG1002, doi:10.1029/2007RG000245.
- Seki, O., T. Nakatsuka, K. Kawamura, S. I. Saitoh, and M. Wakatsuchi (2007), Time-series sediment trap record of alkenones from the western Sea of Okhotsk, *Mar. Chem.*, 104(3–4), 253–265.
- Shabalova, M. V., and G. P. Können (1995), Climate change scenarios: Comparisons of paleoreconstructions with recent temperature changes, *Clim. Change*, 29(4), 409–428.
- Shakun, J. D., P. U. Clark, F. He, S. A. Marcott, A. C. Mix, Z. Liu, B. Otto-Bliesner, A. Schmittner, and E. Bard (2012), Global warming preceded by increasing carbon dioxide concentrations during the last deglaciation, *Nature*, 484(7392), 49–54.
- Shukla, S. P., M. A. Chandler, J. Jonas, L. E. Sohl, K. Mankoff, and H. Dowsett (2009), Impact of a permanent El Niño (El Padre) and Indian Ocean Dipole in warm Pliocene climates, *Paleoceanography*, 24, PA2221, doi:10.1029/2008PA001682.
- Sicre, M. A., Y. Ternois, M. Paterne, A. Boireau, L. Beaufort, P. Martinez, and P. Bertrand (2000), Biomarker stratigraphic records over the last 150 kyears off the NW African coast at 25 degrees N, *Org. Geochem.*, 31(6), 577–588.
- Sirocko, F., M. Claussen, T. Litt, and M. F. Sanchez-Goni (2007), *The Climate of Past Interglacials, Developments in Quaternary Science*, 622 pp., Elsevier, Oxford, U. K.
- Telford, R., C. Li, and M. Kucera (2013), Mismatch between the depth habitat of planktonic foraminifera and the calibration depth of SST transfer functions may bias reconstructions, *Clim. Past*, 9(2), 859–870.
- Tingley, M. P., and P. Huybers (2010), A Bayesian algorithm for reconstructing climate anomalies in space and time. Part I: Development and applications to paleoclimate reconstruction problems, *J. Clim.*, 23(10), 2759–2781.
- Tingley, M. P., P. F. Craigmile, M. Haran, B. Li, E. Mannshardt, and B. Rajaratnam (2012), Piecing together the past: Statistical insights into paleoclimatic reconstructions, *Quat. Sci. Rev.*, 35, 1–22, doi:10.1016/j.quascirev.2012.01.012.

- Villanueva, J., J. O. Grimalt, E. Cortijo, L. Vidal, and L. Labeyrie (1998), Assessment of sea surface temperature variations in the central North Atlantic using the alkenone unsaturation index U_{37}^k , *Geochim. Cosmochim. Acta*, *62*(14), 2421–2427.
- Weaver, P. P. E., L. Carter, and H. L. Neil (1998), Response of surface water masses and circulation to Late Quaternary climate change east of New Zealand, *Paleoceanography*, *13*(1), 70–83.
- Weaver, P. P. E., M. R. Chapman, G. Eglinton, M. Zhao, D. Rutledge, and G. Read (1999), Combined coccolith, foraminiferal, and biomarker reconstruction of paleoceanographic conditions over the past 120 kyr in the northern North Atlantic (59 degrees N, 23 degrees W), *Paleoceanography*, *14*(3), 336–349.
- Wei, G. J., W. F. Deng, Y. Liu, and X. H. Li (2007), High-resolution sea surface temperature records derived from foraminiferal Mg/Ca ratios during the last 260 ka in the northern South China Sea, *Palaeogeogr. Palaeoclimatol. Palaeoecol.*, *250*(1–4), 126–138.
- Weldeab, S., R. R. Schneider, and M. Kolling (2006), Comparison of foraminiferal cleaning procedures for Mg/Ca paleothermometry on core material deposited under varying terrigenous-input and bottom water conditions, *Geochem. Geophys. Geosyst.*, *7*, Q04P12, doi:10.1029/2005GC000990.
- Weldeab, S., R. R. Schneider, and P. Muller (2007a), Comparison of Mg/Ca- and alkenone-based sea surface temperature estimates in the fresh water-influenced Gulf of Guinea, eastern equatorial Atlantic, *Geochem. Geophys. Geosyst.*, *8*, Q05P22, doi:10.1029/2006GC001360.
- Weldeab, S., D. W. Lea, R. R. Schneider, and N. Andersen (2007b), 155,000 years of West African monsoon and ocean thermal evolution, *Science*, *316*(5829), 1303–1307, doi:10.1126/science.1140461.
- Werner, J. P., and M. P. Tingley (2015), Technical note: Probabilistically constraining proxy age-depth models within a Bayesian hierarchical reconstruction model, *Clim. Past*, *11*(3), 533–545.
- Yamamoto, M., T. Oba, J. Shimamune, and T. Ueshima (2004), Orbital-scale anti-phase variation of sea surface temperature in mid-latitude North Pacific margins during the last 145,000 years, *Geophys. Res. Lett.*, *31*, L16311, doi:10.1029/2004GL020138.
- Yamamoto, M., M. Yamamuro, and Y. Tanaka (2007), The California current system during the last 136,000 years: Response of the North Pacific High to precessional forcing, *Quat. Sci. Rev.*, *26*(3/4), 405–14.
- Zachos, J. C., L. D. Stott, and K. C. Lohmann (1994), Evolution of early Cenozoic marine temperatures, *Paleoceanography*, *9*(2), 353–87.
- Zhao, M. X., C. Y. Huang, C. C. Wang, and G. J. Wei (2006), A millennial-scale U_{37}^k sea-surface temperature record from the South China Sea (8 degrees N) over the last 150 kyr: Monsoon and sea-level influence, *Palaeogeogr. Palaeoclimatol. Palaeoecol.*, *236*(1–2), 39–55.